Proton transfer dynamics following strong-field ionization of the water dimer

C. Zhang
School of Science, Nanjing University of Science and Technology, Xiaolingwei 200, 210094 Nanjing, China
and Max-Born-Institut für Nichtlineare Optik und Kurzzeitspektroskopie, Max-Born-Straße 2A, 12489 Berlin, Germany

J. Lu
School of Science, Nanjing University of Science and Technology, Xiaolingwei 200, 210094 Nanjing, China

T. Feng
Max-Born-Institut für Nichtlineare Optik und Kurzzeitspektroskopie, Max-Born-Straße 2A, 12489 Berlin, Germany
and School of Information Science and Engineering, Shandong University, 266237 Qingdao, China

H. Rottke
Max-Born-Institut für Nichtlineare Optik und Kurzzeitspektroskopie, Max-Born-Straße 2A, 12489 Berlin, Germany

(Received 15 January 2019; published 7 May 2019)

Proton transfer is a common process occurring in biologic tissues and chemical reactions involving water which evolves on the femtosecond timescale. We induce and investigate proton transfer through strong-field ionization of isolated water dimers using ultrashort intense laser pulses. Ionization gives rise to ionic molecular dynamics which terminates in proton transfer and dissociation of the singly charged ion, but also in undissociated $(H_2O)_2^+$ ions. Double ionization allows us to experimentally determine the proton transfer rate in $(H_2O)_2^+$ in the electronic ground state.

DOI: 10.1103/PhysRevA.99.053408

I. INTRODUCTION

Hydrogen-bonded systems have attracted considerable interest owing to their important role for the existence of life, chemical reactions, and atmospheric science. For example, hydrogen bonds make the double-helix structure of DNA. Loss of an electron from DNA as a result of ionization can facilitate proton transfer, which is responsible for some biologic functions of DNA [1,2]. The water dimer $(H_2O)_2$ is one of the simplest hydrogen-bonded systems. Many investigations of proton transfer have chosen it as the model molecule. The transfer of a proton between water molecules is an ultrafast process. The timescale in the liquid phase has been estimated from experiments and calculations to be less than 100 fs [3] or even 50 fs [4]. However, there are insufficient experimental data available to date since a direct identification of the H_3O^+ ion in the liquid has remained ambiguous.

The elementary proton transfer can be studied using isolated water dimers $(H_2O)_2$ in the gas phase. It is triggered by photoionization. Vertical photoionization results in a dimer ion substantially off its minimum-energy conformation with the proton not yet transferred. This means that after photoionization, nuclear dynamics starts with the excess energy redistributed among the different degrees of freedom of the ion. This dynamical evolution may result in a persisting rearrangement of the nuclei closer to the equilibrium conformation or, depending on the excess energy, in dissociation, either before or after the proton has been transferred.

Potential-energy surface and molecular dynamics calculations have identified two stable bound ionic equilibrium conformations, one with a transferred proton $(H_3O)^+ - OH$ and one that is hemibonded $(H_2O - OH_2)^+$ with the bond established between the two oxygen atoms [5–8]. Experimentally observed patterns of infrared transitions in the dimer ion combined with a theoretical analysis unambiguously establish that this species is actually best described as the $(H_3O)^+ - OH$ ion radical complex [9].

The dimer ion has two energetically closely spaced electronic states at the ionization threshold of the dimer: the ground state $^2A''$ and the first-excited state $^2A'$ (see, for example, Refs. [6,10,11]). Removing an electron from the $1b_1$ oxygen lone-pair orbital of the proton donor H_2O molecule results in the dimer ion formed in the electronic ground state, while removing it from the oxygen lone-pair orbital of the proton acceptor molecule leaves the dimer ion mainly in the first-excited $^2A'$ electronic state. Theoretical investigations indicate that after photoionization of the neutral dimer, proton transfer in these two electronic states proceeds on different timescales [6,12,13]. For the $^2A''$ electronic ground state, less than 100 fs [12,13] or an even shorter time window (25–50 fs [6,14]) have been found. By contrast, the proton transfer in the $^2A'$ electronic state is expected to take more than 100 fs [12,13] or even at least 300 fs [6] to be completed. Experimental results regarding the timescale it takes for the proton to be transferred are lacking. A recent experiment done by removing an oxygen inner valence shell electron from the water dimer and looking for interatomic Coulombic decay (ICD) only found Coulomb explosion in two H_2O^+ ions after ICD [15]. This means that no proton transfer happened in the time interval between photoionization of the dimer and the ejection of the second electron in the ICD process. ICD thus must proceed significantly faster than proton transfer

 ©2019 American Physical Society

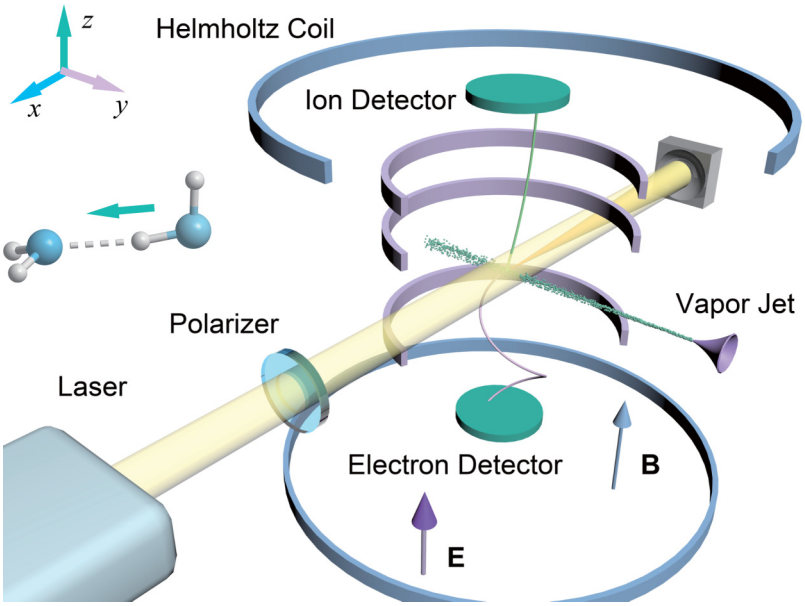

FIG. 1. Sketch of the experimental setup. Guided by an electric (E) and a magnetic (B) field, ions and electrons formed in the focal spot of the laser beam are directed to two position-sensitive multichannel-plate (MCP) detectors. The insets illustrate the possible proton transfer in the $(H_2O)_2^+$ ion and the axis system used in the text.

in the singly charged dimer ion. This result only poses a qualitative lower limit on the time it takes for the proton transfer. Moreover, the photoionization did not remove an electron from one of the outermost valence orbitals of the dimer. This may have a considerable impact on the proton transfer time, as calculations have shown [6,12,13].

We investigated the ionic proton transfer by triggering it via strong-field ionization (SFI) of the water dimer using ultrashort near-infrared laser pulses. This ionization scheme removes an electron from the dimer valence shell, preferentially from the least bound $1b_1$ lone-pair orbital of the proton donor or acceptor water molecule. Besides these ionization pathways, the removal of an electron from one of the two monomer $3a_1$ orbitals may also contribute to SFI in the 10^{14} W/cm^2 light-intensity range [16,17]. Following single ionization, double ionization (DI) is also possible within the same laser pulse. Similar to noble-gas dimers, where the ionization thresholds of the dimer and of the singly charged dimer ion are not very different, both of these sequential ionization steps are expected to proceed via tunnel ionization in the electric field of the laser pulse [18,19]. In between these two SFI steps, a proton transfer in the singly charged ion can happen. In the case of a transfer, double ionization (DI) is expected to result in Coulomb explosion of the doubly charged ion into an $(H_3O)^+$ and an OH^+ ion. Otherwise, Coulomb explosion into two $(H_2O)^+$ ions will occur. The branching ratio into these two Coulomb explosion channels can be used to infer the rate or time constant of the proton transfer. In the experiment, we are able to discern these two DI channels using cold-target recoil ion momentum spectroscopy (COLTRIMS) (see, for example, [20]).

II. EXPERIMENTAL SETUP

The experimental setup consisted of a cold-target recoil ion momentum spectrometer (for more details, see [20,21]). It allows the determination of the three-dimensional momentum vector of individual electrons and ions formed, in our case, in the focal spot of an infrared (IR) laser beam. A schematic view of this setup is shown in Fig. 1. Water dimers formed in a supersonic expansion of water vapor mixed with a carrier gas consisting of Ar and Ne ([Ne]/[Ar] = 4) through a nozzle with an opening of 20 μm in diameter. The total backing pressure behind the nozzle was 2 bar. With the liquid water reservoir and the carrier gas at room temperature, the water vapor partial pressure in the gas mixture amounted to 24 mbar. The chosen expansion conditions led to a dimer fraction $[(H_2O)_2]/[H_2O]$ of less than 1% in the supersonic beam and constrained the formation of larger water clusters. After skimming and collimation, the supersonic jet was crossed by a focused, pulsed Ti:sapphire laser beam (wavelength λ = 780 nm, pulse repetition rate 3 kHz) at right angles (Fig. 1). The light intensity reached in the focal spot was determined to be $(1.2 \pm 0.2) \times 10^{14}$ W/cm^2 with the light pulses having a full width at half maximum of $\tau = 38 \pm 2$ fs. We determined the light intensity from the position of the $10U_p$ cutoff of the kinetic-energy distribution of rescattered photoelectrons emerging from strong-field single ionization of the water monomer molecules in the supersonic beam [22,23]. Here, U_p represents the ponderomotive energy of a free electron in the laser beam. Focusing of the laser beam was accomplished by an on-axis spherical mirror with 150 mm focal length.

Ions and photoelectrons generated in the interaction of the intense light pulses with the atoms and molecules in the supersonic jet were guided by homogenous, parallel electric ($|\mathbf{E}|$ = 630 V/m) and magnetic fields ($|\mathbf{B}| = 3.2 \times 10^{-4}$ T) fields to microchannel-plate (MCP) detectors (diameter 80 mm) equipped with position-sensitive delay-line anodes. The direction of the accelerating electric field was aligned parallel to the direction of the linear polarization of the laser beam.

In an offline analysis, individual ion and photoelectron momenta were determined from the measured times of flight to and hit positions on the MCP detectors. For correlating ions and photoelectrons to individual photoionization and dissociation events, momentum conservation of these processes has been utilized. The COLTRIMS setup used in this experiment approximates to a high degree of accuracy a Wiley-McLaren configuration along the flight path of the ions [24]. This gives

rise to a simple relation between the time of flight of an ion and its momentum component p_z along the extracting electric field (the COLTRIMS axis), which is

$$t_{\mathrm{TOF}} = t^0_{\mathrm{TOF}} - \frac{p_z}{qE} + o\big(p_z^4\big), \tag{1}$$

with $t^0_{\mathrm{TOF}} = \sqrt{8ml_a/qE}$ the time of flight of ions with $p_z = 0$. Here, m is the mass and q is the charge of the ion, E is the electric field strength at the focal spot, and l_a is the effective length of the path where the ion is accelerated. Over the range of ion momenta p_z relevant in this experiment, the corrections to the linear relation between t_{TOF} and p_z, which are of the order of p_z^4, are negligibly small.

Coulomb explosion of a molecular species AB after double ionization in the laser pulse,

$$AB \rightarrow A^+ + B^+ + 2e, \tag{2}$$

can most easily be identified on the basis of momentum conservation along the z axis via p_z of the ions and electrons,

$$0 \approxeq p_z(AB) = p_z(A^+) + p_z(B^+) + p_z(e_1) + p_z(e_2), \tag{3}$$

where $p_z(e_i)$ $(i = 1, 2)$ are the momenta of the two leaving photoelectrons, $p_z(A^+, B^+)$ are the ion momenta, and $p_z(AB)$ is the z component of the momentum of the molecule in the supersonic beam before ionization, which, being perpendicular to the jet axis, can be assumed to be practically zero. The sum momentum of the two ions therefore just equals the recoil momentum imposed by the two leaving photoelectrons, which typically is small compared to the momentum release in the ionic Coulomb explosion. In a plot of $t_{\mathrm{TOF}}(A^+)$ over $t_{\mathrm{TOF}}(B^+)$, ion pairs related to Coulomb explosion thus appear, according to relation (1) between t_{TOF} and p_z, narrowly distributed along a straight line.

For the photoelectrons, the relation between their time of flight (TOF) and the momentum component p_z deviates from a linear relation, especially for large p_z. It can be written as

$$t_{\mathrm{TOF}} = t^0_{\mathrm{TOF}} + \frac{p_z}{qE} + f\big(p_z^2\big), \tag{4}$$

where q is the absolute value of the electron charge, t^0_{TOF} is the electron TOF for $p_z = 0$, and f is a function that depends on the square of p_z. The contribution of $f(p_z^2)$ to t_{TOF} is not negligible, but tends to zero for small p_z.

For single ionization of an atom or molecule in the laser pulse ($A \rightarrow A^+ + e$), one gets, by subtracting the TOF of the electron from that of the singly charged ion,

$$\begin{aligned} &t_{\mathrm{TOF}}(A^+) - t_{\mathrm{TOF}}(e) \\ &\approxeq t^0_{\mathrm{TOF}}(A^+) - t^0_{\mathrm{TOF}}(e) - \frac{p_z(A^+) + p_z(e)}{qE_0} - f\big[p_z^2(e)\big] \\ &= t^0_{\mathrm{TOF}}(A^+) - t^0_{\mathrm{TOF}}(e) - f\big[p_z^2(e)\big] \\ &\approxeq t^0_{\mathrm{TOF}}(A^+) - t^0_{\mathrm{TOF}}(e), \end{aligned} \tag{5}$$

since $p_z(A^+) + p_z(e) = p_z(A) \approxeq 0$ in our experimental setup and the contribution of $f[p_z^2(e)]$ to the TOF difference is typically small. Thus, calculating for each detected ion and photoelectron their TOF difference and filling this result into a histogram will result in narrow peaks for all pairs corresponding to an ionization event $A \rightarrow A^+ + e$. We will exploit this fact for the identification of the ionization processes contributing to the formation of ions and photoelectrons in the experiment.

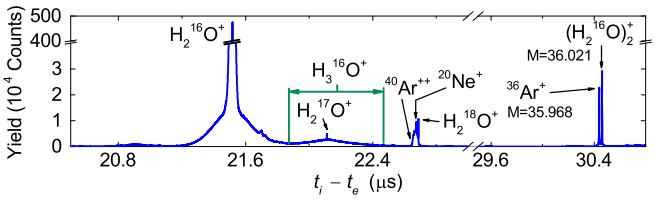

FIG. 2. Histogram of the TOF differences, $t_{\mathrm{TOF}}(I) - t_{\mathrm{TOF}}(e)$, for all ion-photoelectron (I-e) pairs detected in each laser pulse. For pairs from events representing single ionization, this histogram is a high-resolution TOF mass spectrum [see relation (5)]. Besides contributions from the ionization of $H_2{}^{16}O$ (main peak) and of $(H_2O)_2$, ionization of the carrier gases Ar and Ne is found as narrow lines. Stretching the range from at least 21.8 to 22.6 μs H_3O^+ ions contribute to the broad structure found there in the TOF spectrum. The narrow peak on top of this structure represents ionization of $H_2{}^{17}O$.

III. RESULTS AND DISCUSSION

A. Protonated and unprotonated Coulomb explosion

Figure 2 shows a histogram detail of the TOF differences of all possible combinations of ion-photoelectron (I-e) pairs detected in each laser pulse. According to relation (5) above, these time differences represent a high-resolution TOF mass spectrum for singly ionized species related to ionization processes $A \rightarrow A^+ + e$, where A may be any atom or molecule. The most prominent feature in the time window shown is the narrow H_2O^+ ion peak at $t_i - t_e = 21.52$ μs, which is sitting on top of a broader background feature extending from $\approx$21.24 to $\approx$21.8 μs. The narrow H_2O^+ line is related to the ionization process $H_2O \rightarrow H_2O^+ + e$ of water molecules in the supersonic jet (with O being the ^{16}O isotope), whereas the broad feature beneath is related to the ionization of water molecules present in the residual background gas in the vacuum chamber. Unlike the molecules in the jet, they have a thermal velocity distribution corresponding to room temperature ($T \approx 293$ K) and thus give rise to a broader $t_i - t_e$ distribution. A second contribution possibly arising from dissociative single ionization of water dimers [$(H_2O)_2 \rightarrow H_2O + H_2O^+ + e$], where the H_2O^+ ion picks up momentum from dissociation, can be ruled out.

Dissociative ionization of $(H_2{}^{16}O)_2$ dimers,

$$(H_2{}^{16}O)_2 \rightarrow {}^{16}OH + (H_3{}^{16}O)^+ + e, \tag{6}$$

forms the broad feature appearing between $\approx$21.65 μs and $\approx$22.6 μs, while the narrow line on top of it at $t_i - t_e = 22.11$ μs is stemming from the single ionization of $H_2{}^{17}O$ molecules present in the jet. The presence of $(H_3{}^{16}O)^+$ ions indicates that strong-field ionization of the dimer reaches ionic electronic states which dissociate after a proton transfer into an OH radical and a protonated water molecule. Besides this channel, undissociated dimer ions are also found (the line at $t_i - t_e = 30.46$ μs in the histogram in Fig. 2), formed in the

strong-field ionization process,

$$(H_2{}^{16}O)_2 \rightarrow (H_2{}^{16}O)_2{}^+ + e. \quad (7)$$

These dimer ions may either exist as a protonated water molecule $(H_3O)^+$ bound to an OH radical or as a water ion $(H_2O)^+$ bound to a neutral water molecule. Since strong-field ionization (SFI) most probably removes an electron from the highest occupied molecular orbital (HOMO) $2a''$ of the water dimer, the ion is mainly left behind in the electronic ground state $1^2A''$ [11,25,26]. However, the first-excited ionic state $1^2A'$ has an excitation energy of only 1.1 eV above the ground state. Therefore, this state may also become populated after SFI [10]. Similar to one-photon ionization, SFI proceeds vertically as a Franck-Condon transition. Therefore, both ionic states are reached off the equilibrium nuclear configuration, which for both states corresponds to a proton-transferred conformation without any barrier to overcome [26]. Molecular dynamics simulations after vertical ionization of water dimers indicate that a permanent proton transfer can be expected after removal of an electron from the water $1b_1$, $3a_1$, or $1b_2$ valence orbitals, independent of whether the electron is removed from the donor or acceptor H_2O moiety [12]. Removal of the electron from the donor water molecule $1b_1$ HOMO is related to forming the dimer ion in the electronic ground state $1^2A''$, whereas the removal of the electron from the acceptor $1b_1$ HOMO is related to forming the dimer ion in the excited electronic state $1^2A'$.

Deeper insight into the role that proton transfer plays after SFI of the water dimer can be gained from looking into strong-field double ionization of the dimer within the laser pulse. It will also give a clue to how fast the proton transfer proceeds. Depending on the position of the proton, there are two possible results of the second ionization step,

$$(H_3O)^+ - OH \rightarrow (H_3O)^+ + (OH)^+, \quad (8)$$

$$(H_2O)^+ - H_2O \rightarrow (H_2O)^+ + (H_2O)^+, \quad (9)$$

with the two positive charges repelling each other and thus terminating in Coulomb explosion of the two charged entities. Double ionization accompanied by Coulomb explosion can be identified according to relations (1) and (3) above in a two-dimensional histogram where every entry represents the TOFs of ion pairs detected in each laser pulse. Figure 3(a) shows a cutout of this histogram covering the TOF range where ion pairs from the Coulomb explosion channels (8) and (9) above are expected to be found. The recorded TOFs of these ion pairs appear along the two closely spaced straight lines shown in the correlation spectrum [Fig. 3(a)]. Stretching along these lines, we find three accumulation points of ion pairs close to the times of flight of the first ion of 20 750, 20 250, and 19 600 ns.

In order to focus on proton transfer in the dimer ion, Fig. 3(b) zooms further into the Coulomb explosion channels (8) and (9). Different from Fig. 3(a), now on the vertical axis the sum of the times of flight of the ion pairs, $t_1 + t_2$, is shown, whereas along the horizontal axis again the TOF t_1 of the first ion reaching the ion detector is plotted. According to the relations (1), (3), and (4) above, the distribution of ion pairs along the vertical axis closely represents the recoil of these

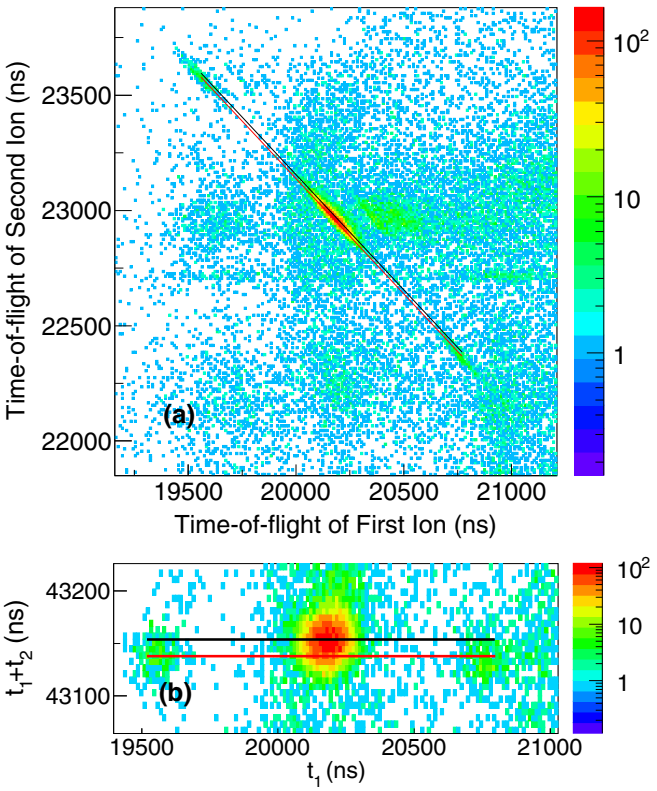

FIG. 3. (a) Correlation histogram of the times of flight of ion pairs evaluated for all laser pulses where at least two ions have been detected. The two closely spaced black and red lines indicate the positions where ion pairs from protonated [channel (8)] and unprotonated [channel (9)] Coulomb explosions, respectively, are expected. The bin size of the histogram is 10 × 10 ns. (b) Correlation histogram of the time of flight t_1 of the first ion detected and the time-of-flight sum $t_1 + t_2$ of the ion pairs in (a). The bin size of this histogram is 6 × 6 ns.

pairs in the Coulomb explosion channels (8) and (9) due to the emission of the two photoelectrons.

The two straight lines shown in Fig. 3(a) map onto the two horizontal lines in Fig. 3(b). The higher time resolution now clearly differentiates the two lines from each other. The black one passes through the vertical center of the central accumulation point of ion pairs and the red one through the centers of the pair of accumulation points to the left and to the right.

The black and red lines have been calculated assuming the two photoelectrons leaving after double ionization have zero sum momentum along the z axis. Then relations (1) and (3) for the times of flight for ions results in

$$t_{\mathrm{TOF}}(A^+) + t_{\mathrm{TOF}}(B^+) \approxeq t^0_{\mathrm{TOF}}(A^+) + t^0_{\mathrm{TOF}}(B^+), \quad (10)$$

that is, in a constant value for ions emerging from Coulomb explosion. The actual sum-momentum distribution of the two photoelectrons along the z axis is represented by the extension of the three ion-pair accumulation points along the vertical axis of Fig. 3(b).

In an ion TOF spectrum, the center of the line $t^0_{\mathrm{TOF}}(H_2O^+)$ corresponding to water ions formed by SFI of water molecules is located at $t^0_{\mathrm{tof}} = 21\,578$ ns. It corresponds to H_2O^+ ions

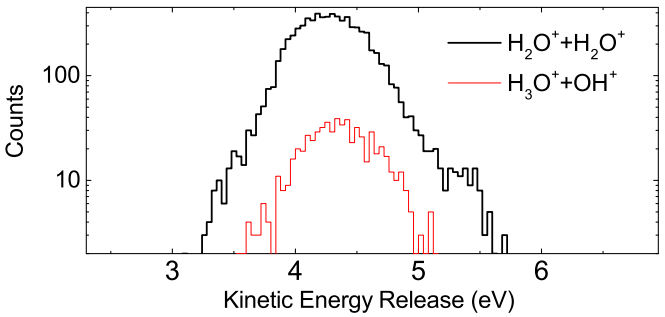

FIG. 4. Measured KER of the ions after Coulomb explosion of the dimer into $H_2O^+ + H_2O^+$ (black line) and $H_3O^+ + OH^+$ (thin red line) following strong-field double ionization of water dimers.

with zero momentum along the z axis [$p_z = 0$; see relation (2) and Fig. 1 for the direction of the z axis]. Therefore, the center of the sum of the TOFs (10) for unprotonated ion fragment pairs from the Coulomb explosion channel (9) appears at $t^0_{\mathrm{TOF}} = 43\,156$ ns. This is just the position of the black line in Fig. 3(b). The central accumulation point of ions thus represents unprotonated ion pairs emerging from the Coulomb explosion channel (9).

The red line in Fig. 3(b), passing through the centers of the two ion-pair accumulation points to the left and right of the center one, is clearly offset from the black line by −17 ns. This means these two accumulation points do not correspond to the Coulomb explosion channel (9). The analysis of this offset using relation (10) reveals that these two ion-pair accumulation points correspond to the protonated Coulomb explosion channel (8). The left accumulation point can be identified to be OH^+ and the right one to be H_3O^+ ions associated with the explosion channel (8).

Based on this analysis, kinetic-energy release (KER) spectra can be calculated for the Coulomb explosion channels (8) and (9). Figure 4 shows these spectra. The red line corresponds to channel (8) and the black one to the unprotonated channel (9). The branching ratio R_p into the protonated Coulomb explosion channel (8) amounts to $R_p = Y_p/(Y_p + Y_u) = 0.081 \pm 0.003$, where Y_p and Y_u are the total ion yields in the protonated (8) and in the unprotonated (9) channel.

The distribution centers for the KER are found at 4.35 eV [channel (8)] and 4.27 eV [channel (9)] with the widths of both distributions (full width at half maximum) $\Delta E \approx 0.7$ eV being approximately equal. For the unprotonated channel (9), the KER distribution that we find agrees well with the one observed in Ref. [15] for this channel after intermolecular Coulombic decay initiated by photoionizing an electron from the ($2s$) orbital of one of the oxygen atoms. In Ref. [15], the center of the distribution is located at 4.15 eV with a full width at half maximum $\Delta E = 0.95$ eV which is slightly larger than the one we measured. The maximum appears by 0.12 eV offset to lower KER from the one we found. Small distinct differences in the KER distributions may have their origin in the fact that the KER distribution in Ref. [15] maps the complete 4π solid-angle range, while our distribution is limited to a small solid angle along the direction of linear polarization of the laser beam (polar angle range $0 \leqslant \theta \leqslant 20 \pm 2$ deg, with ±2 deg accounting for its variation over the KER range of the Coulomb explosion products in Fig. 4). The protonated Coulomb explosion channel (8) has not been observed in Ref. [15].

From the KER distribution centers and from their widths, it is possible to estimate the distance R between the two positive charge centers, which repel each other, and the width of the charge separation distributions where the Coulomb explosion starts. Assuming the starting kinetic energy is zero and the repulsive potential can be approximated by simple Coulomb repulsion of two point charges $V(R) = 1/R$, one arrives at $R = 6.25$ a.u. ($\Delta R = 1.0$ a.u.) for the Coulomb explosion channel (8) and at $R = 6.4$ a.u. ($\Delta R = 1.0$ a.u.) for the unprotonated channel (9). The widths ΔR given are the full widths at half maximum.

The charge center separation obtained for the unprotonated Coulomb explosion channel (9) (center of the KER distribution) is 0.89 a.u. larger than the O−O equilibrium separation R_e in the neutral dimer in the electronic ground state ($R_e = 5.51$ a.u. [6,27]). Provided that the two photoelectrons are removed from the lone-pair orbitals of the two oxygen atoms of the dimer, one would expect an initial charge center separation close to the O−O separation. The mismatch we find may be for two reasons. If the simple Coulomb repulsion used for the relation between the KER and the charge separation applies, the difference may mean that the two charge centers are not located exactly on the two oxygen nuclei or some nuclear motion happened before the second electron was removed from the still neutral site of the dimer. On the other hand, simple Coulomb repulsion may not correctly describe the interaction potential at small O−O separations where the Coulomb explosion starts. This would mean the simple relation used to calculate the charge center separation would not apply.

For the protonated Coulomb explosion channel (8), it is not possible to obviously locate the charge centers in the H_3O^+ and OH^+ moieties at the starting point of Coulomb explosion. Assuming simple Coulomb repulsion, the KER suggests a charge center separation of $R = 6.25$ a.u., a value only slightly less than that for the unprotonated explosion and again larger than the equilibrium O−O separation in the neutral dimer. In the electronic ground state of the dimer ion, the proton-oxygen separation in the H_3O^+ entity has been calculated to be 1.96 a.u. and the separation of the proton from the oxygen atom of the OH radical to be 2.68 a.u. directly after proton transfer is completed [6]. If one assumes the positive charge on the H_3O^+ moiety to be located at the transferred proton, and ionization of OH in the second step to proceed by removing an electron from the oxygen atom with the positive charge staying localized there, then the Coulomb explosion cannot start immediately after the proton transfer is finished. If it would and a simple Coulomb repulsion prevails, then the KER would have been 10.15 eV ($R = 2.68$ a.u.), i.e., significantly higher than the measured 4.35 eV. In case a simple Coulomb repulsion prevails, this difference may mean that the positive charge locations immediately after proton transfer are not as assumed above (assumption: the Coulomb explosion starts directly after proton transfer) or the separation between the H_3O^+ and OH entities has increased before ionization of OH starts the Coulomb explosion. Alternatively, basic Coulomb repulsion between H_3O^+ and OH^+ at small

separations between the two ions may be too simple of an assumption. A final answer of how the measured KER after Coulomb explosion is related to the geometry of the dimer ion immediately before the second ionization step needs a deeper knowledge of the positive charge distribution directly after double ionization and of the interaction potential between the two positively charged moieties for the protonated (8) and unprotonated (9) Coulomb explosion channels at small separations.

B. Proton transfer rate

The fact that we observe the protonated Coulomb explosion channel (8) means that the proton transfer has to proceed on the timescale of the duration of the laser pulse used for SFI of the water dimer, i.e., on a timescale of ≈40 fs or less. Actually, theory indicates that in the electronic ground state of the dimer ion $^2A''$ (C_s symmetry assumed), proton transfer is completed in less than 100 fs (≈50 fs) [6,7,13]. The $^2A''$ ion ground state is reached when an electron is removed from the b_1 lone-pair oxygen HOMO of the donor water molecule of the dimer. The first electronically excited state of the dimer $^2A'$ is accessed when an electron is ionized from the same orbital of the acceptor water molecule. For this excited ionic state, and also for higher excited states, theory predicts a significantly slower proton transfer, which takes 150–200 fs to be completed [6,13]. Both of these lowest-lying electronic states may be reached by strong-field ionization of the water dimer. However, one expects the ground state to overwhelmingly contribute to the observed protonated Coulomb explosion channel.

Based on the expectation that the ionic ground state contributes most to the protonated Coulomb explosion channel, we employ a simplified rate model to further quantify the proton transfer rate in the dimer ion. The model employed is illustrated in Fig. 5. The ionization rate $r_1(t)$ of the neutral dimer is approximated by the Ammosov-Krainov-Delone (ADK) strong-field ionization rate assuming that an electron is removed from the lone-pair oxygen orbital of the donor H_2O molecule [28]. The orbital is approximated to be an atomic p orbital ($l = 1$). We further assume that only the $m_l = 0$ component of the p orbital contributes to SFI (the angular momentum quantization axis supposed to be parallel to the polarization vector of the laser pulse). Based on atomic SFI, actually the $m_l = 0$ component of an orbital mainly contributes to the ionization rate. Also the ADK ionization rate in Ref. [28] that we use in the rate model indicates that the two $|m_l| = 1$ magnetic quantum numbers contribute less than ≈6 % to the rate at the light intensity used in our experiment. The rate $r_2(t)$ which characterizes the second ionization step terminating in the unprotonated Coulomb explosion channel (9) is also approximated by a simple ADK rate. In this case, the second electron is removed from the lone-pair oxygen p orbital of the acceptor moiety of the dimer ion. The proton transfer rate $r_{\rm pt}$ is assumed to be a constant. After proton transfer, we also use the ADK rate for the second step ionization rate $r_3(t)$ of the OH radical, again assuming that an electron in the oxygen p orbital gets ionized. This ionization step terminates in the protonated Coulomb explosion channel (8).

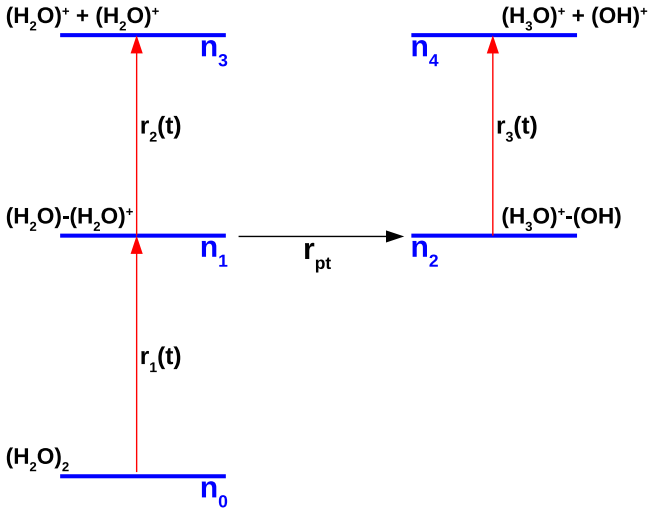

FIG. 5. Model used to analyze the observed strong-field double ionization of $(H_2O)_2$ on the basis of rate equations. The notation is according to the rate equations (11) with $n_i(t)$, $i = 0, \ldots, 4$, representing the probability to find the respective ions as given in the figure. The rates $r_i(t)$, $i = 1, \ldots, 3$, represent the time-dependent ADK ionization rates for the SFI steps involved in double ionization of the dimer. $r_{\rm pt}$ is the time-independent proton transfer rate.

With these ingredients, the rate equation system we use is given by (see Fig. 5 for the notation used)

$$\begin{aligned}
\dot{n}_0 &= -r_0(t)n_0,\\
\dot{n}_1 &= r_0(t)n_0 - [r_2(t) + r_{\rm pt}]n_1,\\
\dot{n}_2 &= r_{\rm pt}n_1 - r_3(t)n_2,\\
\dot{n}_3 &= r_2(t)n_1,\\
\dot{n}_4 &= r_3(t)n_2.
\end{aligned} \tag{11}$$

This set of equations is solved using a sine-squared pulse shape for the electric field strength of the laser pulse with a full width at half maximum (FWHM) of 52 fs and the initial conditions $n_0(0) = 1$ and $n_i(0) = 0$ ($i = 1, \ldots, 4$). This half width corresponds to a FWHM of the light intensity of the pulse of 38 fs as used in the experiment.

The main result of the calculation which can be compared with the experimentally observed branching ratio $R_p = n_4(T)/[n_3(T) + n_4(T)] = 0.081 \pm 0.003$ is shown in Fig. 6. In this figure, the dependence of the calculated ratio $n_4(T)/[n_3(T) + n_4(T)]$ at the end of the laser pulse on the proton transfer rate $r_{\rm pt}$ is shown for three different laser pulse intensities $I = (1.0,\ 1.2,\ 1.4) \times 10^{14}$ W/cm^2 in the transfer rate range up to 0.08 fs^{-1}. The low- and high-intensity curves shown enclose the range of light intensities determined by the error margin with which we know the intensity (see Sec. II for the derivation of the margin). The horizontal dark-gray shaded area centered at $n_4(T)/[n_3(T) + n_4(T)] = 0.081$ shows the measured branching ratio R_p including its error margin. The corresponding proton transfer rate range, assuming a light intensity of 1.2×10^{14} W/cm^2, is covered by the vertical dark-gray shaded area. It is narrower than the rate range limits set by the accuracy with which we know the light intensity (light-gray shaded area). However, as can be seen from the

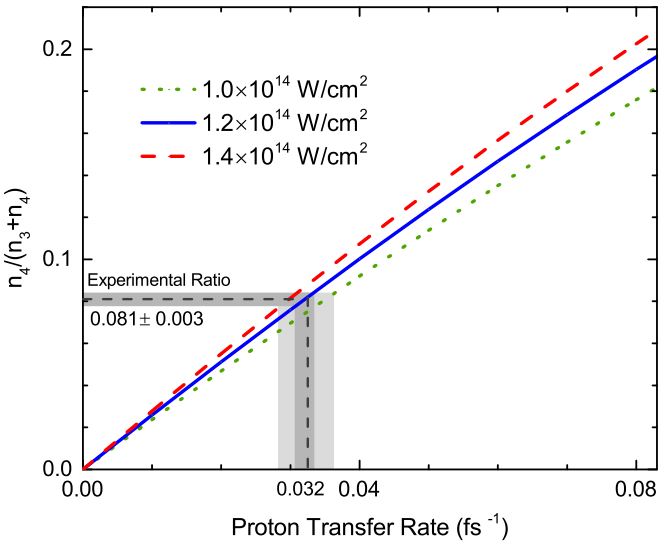

FIG. 6. The ratio $n_4/(n_3+n_4)$ of the probabilities to find ions in the protonated Coulomb explosion channel (8) over the probability to find ions in both the protonated and unprotonated (9) channels at the end of the laser pulse plotted over the proton transfer rate r_{pt}. The three curves correspond to three different light intensities, as stated in the figure. The horizontal line indicates the ratio observed in the experiment.

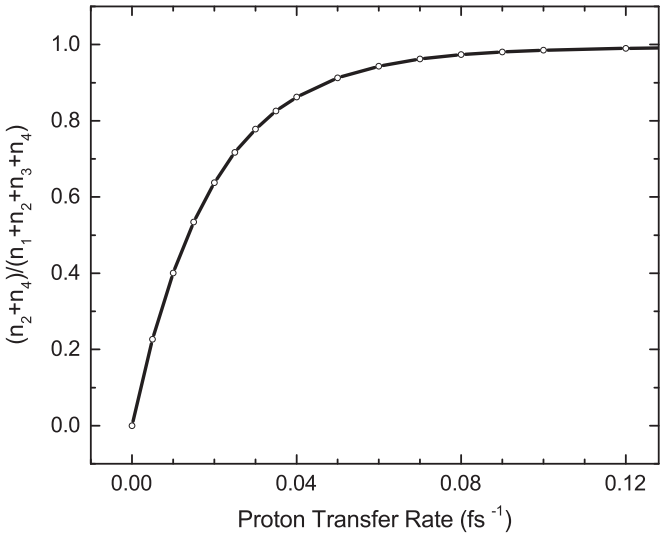

FIG. 7. The ratio $(n_2+n_4)/\sum_{i=1}^{4} n_i$ of the probabilities to find any protonated ions over the probability to find any ions, singly or doubly charged, at the end of the laser pulse plotted over the proton transfer rate r_{pt}. The curve shown has been calculated for the light intensity used in the experiment ($I = 1.2 \times 10^{14}$ W/cm^2). It is a measure of the total proton transfer probability at the end of the laser pulse, i.e., after 104 fs (assumption: the FWHM of the light intensity is 38 fs and the electric field of the pulse follows a sin^2 function as assumed in the calculation).

plot, the measured ratio allows a quite precise determination of the actual proton transfer rate even if one allows for a variation of the laser pulse peak intensity between $I = 1.0 \times 10^{14}$ and $I = 1.4 \times 10^{14}$ W/cm^2. From Fig. 6 (light-gray shaded rate range), one reads a proton transfer rate of $r_{pt} = 0.032 \pm 0.005$ fs^{-1}. The time constant for proton transfer after SFI of the water dimer thus amounts to $\tau_{pt} = 1/r_{pt} = 31 \pm 5$ fs. This time constant is of the order of the laser pulse width of 38 fs. The error margins we give allow for the inaccuracy in the determination of the experimental light intensity.

The time constant for proton transfer that we derive from the experiment can be compared to the results of several molecular dynamics calculations which address the proton transfer starting after ionization of the water dimer in the ion's electronic ground state [6,12,13]. Tachikawa's calculations indicate that proton transfer after ionization is complete within 25–50 fs [6]. Similarly, according to Ref. [12], the proton transfer is complete (probability 1) within 100 fs and with probability 0.8 within ≈50 fs. Both of these theoretical values compare favorably with the transfer time constant that we derive from our experimental result. However, one has to keep in mind that the time constant that we derive from the transfer rate can only represent the mean time it takes for the dimer ion to switch from the unprotonated to the protonated conformation, while molecular dynamics calculations determine the actual time interval for the proton to move between the two positions in the dimer.

From the rate equations we can also derive the quantity $[n_2(T)+n_4(T)]/\sum_{i=1}^{4} n_i(T)$ (see Fig. 5). It measures the ratio of all ions (singly and doubly charged) which have undergone a proton transfer and all singly and doubly charged ions at the end of the sine-squared laser pulse. This ratio is shown in Fig. 7 as a function of the proton transfer rate r_{pt} for a laser pulse intensity of 1.2×10^{14} W/cm^2 used in the experiment. The figure shows that proton transfer in the dimer ion at the end of the laser pulse is complete with a "probability" of ≈0.8 at the experimentally determined transfer rate $r_{pt} = 0.032$ fs^{-1}. The end of the laser pulse means the time when the sine-squared electric field pulse reaches zero (i.e., $T = 104$ fs for the laser pulse with a FWHM of the light intensity of 38 fs). This outcome also compares favorably with the theoretical result derived in Ref. [12] (see the preceding paragraph).

IV. CONCLUSION

In conclusion, strong-field ionization is capable to give deeper insight into the proton transfer dynamics in water dimers which starts after their ionization. We have been able to identify ionic proton transfer using this method and to get an experimental value for the proton transfer rate using strong-field double ionization of the dimer. The experimentally derived rate compares favorably with the theoretical values for the time it takes for the proton transfer in the dimer ion electronic ground state. Since our determined timescale for the transfer is similar to the laser pulse duration, one presently cannot exclude a possible influence of the strong laser field on the transfer rate. One way to eliminate this influence would be a significant reduction of the laser pulse width and the use of two pulses delayed with respect to each other to induce double ionization in a pump-probe experiment. Our derived transfer rate indicates that for such a pump-probe experiment, pulses with a width of ≈10 fs would be necessary to use. Such a pump-probe experiment would also allow investigating, how nuclear dynamics possibly changes the conformation of the

singly charged ion before the second pulse doubly ionizes it. Our results also reveal that stable $(H_2O)_2^+$ ions are formed in SFI which have already been observed to exist after one-photon ionization of the water dimer at low light intensity.

The experimental technique used here can also provide access to molecular dynamics in larger water clusters. It allows one to exploit correlations among the charged particles, electrons and ions, formed in the strong-field interaction process to get a very detailed view of the molecular dynamics starting after ionization. The next bigger cluster ion fragment of importance following $[H_2O]H^+$ would be $[H_2O]_2H^+$, which we also detected in this experimental investigation following SFI presumably of $(H_2O)_3$. Similar to the liquid phase, $[H_2O]_2H^+$ may exist in the Zundel conformation (see, for example, [29]).

ACKNOWLEDGMENTS

T.F. would like to thank the Taishan Young Scholar Program of Shandong Province and Qilu Young Scholar Program of Shandong University for financial support. This work was supported by the National Natural Science Foundation of China under Grant No. 11774176.

[1] A. K. Ghosh and G. B. Schuster, J. Am. Chem. Soc. **128**, 4172 (2006).
[2] A. Kumar and M. D. Sevilla, J. Phys. Chem. B **113**, 11359 (2009).
[3] Y. Gauduel, S. Pommeret, A. Migus, and A. Antonetti, Chem. Phys. **149**, 1 (1990).
[4] A. Furuhama, M. Dupuis, and K. Hirao, J. Chem. Phys. **124**, 164310 (2006).
[5] Q. Cheng, F. A. Evangelista, A. C. Simmonett, Y. Yamaguchi, and H. F. Schaefer III, J. Phys. Chem. A **113**, 13779 (2009).
[6] H. Tachikawa, Phys. Chem. Chem. Phys. **13**, 11206 (2011).
[7] O. Svoboda, M. Ončák, and P. Slavíček, J. Chem. Phys. **135**, 154302 (2011).
[8] D. M. Chipman, J. Phys. Chem. A **120**, 9618 (2016).
[9] G. H. Gardenier, M. A. Johnson, and A. B. McCoy, J. Phys. Chem. A **113**, 4772 (2009).
[10] S. Tomoda, Y. Achiba, and K. Kimura, Chem. Phys. Lett. **87**, 197 (1982).
[11] L. A. Curtiss, Chem. Phys. Lett. **96**, 442 (1983).
[12] O. Svoboda, D. Hollas, M. Ončák, and P. Slavíček, Phys. Chem. Chem. Phys. **15**, 11531 (2013).
[13] J. Chalabala, F. Uhlig, and P. Slavíček, J. Phys. Chem. A **122**, 3227 (2018).
[14] E. Kamarchik, O. Kostko, J. M. Bowman, M. Ahmed, and A. I. Krylov, J. Chem. Phys. **132**, 194311 (2010).
[15] T. Jahnke, H. Sann, T. Havermeier, K. Kreidi, C. Stuck, M. Meckel, M. Schöffler, N. Neumann, R. Wallauer, S. Voss *et al.*, Nat. Phys. **6**, 139 (2010).
[16] J. P. Farrell, S. Petretti, J. Förster, B. K. McFarland, L. S. Spector, Y. V. Vanne, P. Decleva, P. H. Bucksbaum, A. Saenz, and M. Gühr, Phys. Rev. Lett. **107**, 083001 (2011).
[17] S. Petretti, A. Saenz, A. Castro, and P. Decleva, Chem. Phys. **414**, 45 (2013).
[18] B. Manschwetus, H. Rottke, G. Steinmeyer, L. Foucar, A. Czasch, H. Schmidt-Böcking, and W. Sandner, Phys. Rev. A **82**, 013413 (2010).
[19] B. Ulrich, A. Vredenborg, A. Malakzadeh, M. Meckel, K. Cole, M. Smolarski, Z. Chang, T. Jahnke, and R. Dörner, Phys. Rev. A **82**, 013412 (2010).
[20] J. Ullrich, R. Moshammer, A. Dorn, R. Dörner, L. P. H. Schmidt, and H. Schmidt-Böcking, Rep. Prog. Phys. **66**, 1463 (2003).
[21] C. Zhang, T. Feng, N. Raabe, and H. Rottke, Phys. Rev. A **97**, 023417 (2018).
[22] B. Yang, K. J. Schafer, B. Walker, K. C. Kulander, P. Agostini, and L. F. DiMauro, Phys. Rev. Lett. **71**, 3770 (1993).
[23] G. G. Paulus, W. Becker, W. Nicklich, and H. Walther, J. Phys. B: At. Mol. Opt. Phys. **27**, L703 (1994).
[24] W. C. Wiley and I. H. McLaren, Rev. Sci. Instrum. **26**, 1150 (1955).
[25] K. Sato, S. Tomoda, K. Kimura, and S. Iwata, Chem. Phys. Lett. **95**, 579 (1983).
[26] S. Tomoda and K. Kimura, Chem. Phys. **82**, 215 (1983).
[27] H. Tachikawa and T. Takada, RSC Adv. **5**, 6945 (2015).
[28] M. V. Ammosov, N. B. Delone, and V. P. Krainov, Zh. Eksp. Teor. Fiz. **91**, 2008 (1986) [Sov. Phys. JETP **64**, 1191 (1986)].
[29] F. Dahms, B. P. Fingerhut, E. T. J. Nibbering, E. Pines, and T. Elsaesser, Science **357**, 491 (2017).